



No impact of tropospheric ozone on the gross primary productivity of a Belgian pine forest

Lore T. Verryckt¹, Maarten Op de Beeck¹, Johan Neirynck², Bert Gielen¹, Marilyn Roland¹, and Ivan A. Janssens¹

¹Department of Biology, University of Antwerp, Wilrijk 2610, Belgium

²Research Institute for Nature and Forest, Geraardsbergen 9500, Belgium

Correspondence to: Lore T. Verryckt (lore.verryckt@uantwerpen.be)

Received: 12 January 2016 – Discussion started: 23 February 2016

Revised: 2 March 2017 – Accepted: 3 March 2017 – Published: 5 April 2017

Abstract. High stomatal ozone (O_3) uptake has been shown to negatively affect crop yields and the growth of tree seedlings. However, little is known about the effect of O_3 on the carbon uptake by mature forest trees. This study investigated the effect of high O_3 events on gross primary productivity (GPP) for a Scots pine stand near Antwerp, Belgium over the period 1998–2013. Stomatal O_3 fluxes were modelled using in situ O_3 mixing ratio measurements and a multiplicative stomatal model, which was parameterised and validated for this Scots pine stand. Ozone-induced GPP reduction is most likely to occur during or shortly after days with high stomatal O_3 uptake. Therefore, a GPP model within an artificial neural network was parameterised for days with low stomatal O_3 uptake rates and used to simulate GPP during periods of high stomatal O_3 uptake. Possible negative effects of high stomatal O_3 uptake on GPP would then result in an overestimation of GPP by the model during or after high stomatal O_3 uptake events. The O_3 effects on GPP were linked to AOT40 and POD₁. Although the critical levels for both indices were exceeded in every single year, no significant negative effects of O_3 on GPP were found, and no correlations between GPP residuals and AOT40 and POD₁ were found. Overall, we conclude that no O_3 effects were detected on the carbon uptake by this Scots pine stand.

1 Introduction

Tropospheric ozone (O_3) is a secondary air pollutant that has the potential to negatively affect vegetation, leading to reduced growth and carbon sequestration potential (ICP Vegetation, 2011; Subramanian et al., 2015). Background concen-

trations of tropospheric O_3 have increased 30 % since pre-industrial times (Young et al., 2013) and are projected to further increase considerably until about 2050 (IPCC, 2007). Depending on the scenarios, background O_3 levels might either increase or decrease after 2050 (IPCC, 2007).

In recent years, many studies have been conducted to investigate the mechanisms underlying the O_3 impacts on vegetation. Ozone reduces plant growth by altering photosynthetic rates, carbohydrate production, carbon sequestration, carbon allocation, and carbon translocation (Beedlow et al., 2004; Ashmore, 2005; Wittig et al., 2009). Once O_3 enters the leaves through the stomata, it can affect plant growth through direct cellular damage (Mauzerall and Wang, 2001), leading to visible leaf injury and reduced leaf longevity (Li et al., 2016). In response to O_3 , respiratory processes increase, which will also affect the tree's carbon balance (Ainsworth et al., 2012). Skärby et al. (1987) proved that the dark respiration of Scots pine shoots increased after long-term exposure to a low level of O_3 . Protective responses, such as compensation (e. g. repair of injured tissue), avoidance (e. g. stomatal closure), and tolerance (e. g. alteration of metabolic pathways), all consume carbon; hence, resistance to O_3 damage costs energy. The size of this cost affects the amount of carbon remaining to support growth (Skärby et al., 1998).

To assess the impact of O_3 , several indices have been created: AOT40 (ppb h), the cumulative O_3 mixing ratio in excess of a threshold of 40 ppb, and POD_y, the accumulated O_3 flux above a flux threshold y ($\text{nmol m}^{-2} \text{s}^{-1}$). Critical levels are quantitative estimates of exposure to O_3 above which direct adverse effects may occur (CLRTAP, 2015); these have been determined for the indices based on O_3 dose-response relationships from fumigation experiments with enhanced O_3

mixing ratios (Karlsson et al., 2004). The magnitude of the O₃ impact on plants depends on the intensity of O₃ exposure, environmental factors influencing both plant photosynthesis and the O₃ flux to plant surfaces, and plant species-specific defensive mechanisms (Musselman and Massman, 1999). Because of the variable plant responses to similar O₃ mixing ratios, the question arises as to whether widely applicable tolerable limits of O₃ mixing ratios exist (Skärby et al., 1998).

While high stomatal O₃ fluxes have been shown to affect the yield of crops and the growth of tree seedlings and saplings (e.g. Büker et al., 2015), little is known about the effect on mature forest trees. When scaling up the results from seedlings to mature trees, the resulting data should be viewed with caution due to differences in energy budgets, canopy : root balances, and architecture and carbon allocation patterns (McLaughlin et al., 2007; Huttunen and Manninen, 2013). In addition to the uncertainties related to the up-scaling from seedlings to mature trees, data from controlled experiments should also be used with caution because trees can react differently in field conditions (Skärby et al., 1998). The effect of O₃ uptake on carbon uptake under ambient O₃ mixing ratios by trees has hardly been studied in situ. Some studies showed reductions in plant growth due to stomatal O₃ uptake (Zapletal et al., 2011; Fares et al., 2013; Yue and Unger, 2014), while other studies did not show any effect (Samuelson, 1994; Zona et al., 2014). The presence of a stomatal O₃ uptake effect was found to be species- and site-specific, and there is a clear need for more studies investigating the effect of O₃ on carbon uptake by mature trees in the field (Huttunen and Manninen, 2013).

In this study, we investigated the effect of O₃ at ambient levels on the gross primary productivity (GPP) of a mature Scots pine stand in Flanders, Belgium over a period of 14 growing seasons between 1998 and 2013. The investigation of O₃ effects on GPP is relevant because GPP represents the first step in the process of C assimilation and quantifies the rate at which C substrate is provided for growth, wood production, et cetera. Critical levels of AOT40 and POD₁ are being exceeded for this stand (Neirynck et al., 2012), indicating a potential effect of O₃ on tree productivity already at current ambient levels. To detect O₃ effects on GPP, we adopted a modelling approach that involved simulating GPP with a model with an O₃-damage-free parameterisation and evaluating model overestimations of GPP. We used an artificial neural network (ANN) to model GPP. ANNs are a power tool to process multidimensional data in which complex non-linear interrelationships between the parameters can be expected. ANNs are successfully used in remote sensing, evolutionary ecology, et cetera, and have previously been used to model GPP (Lek and Guegan, 1999; Rochelle-Newall et al., 2007; Akhand et al., 2016; Liu et al., 2016). In this study, we used ANNs since they do not employ predefined model conditions compared to conventional statistical models.

2 Materials and methods

2.1 Study area

The study area consisted of a 2 ha Scots pine stand in a 150 ha coniferous and deciduous forest named “De Inslag”, situated in Brasschaat (+51°18'33" N, +04°31'14" E) northeast of the Antwerp agglomeration and east-northeast of the Antwerp harbour (Neirynck et al., 2008). The site has a temperate maritime climate with a mean annual temperature of 11 °C and a mean annual precipitation of 830 mm (Neirynck et al., 2008). The soil has been classified as Albic Hypoluvic Arenosol (Gielen et al., 2011), a moderately wet sandy soil with a distinct humus and/or iron B horizon (Janssens et al., 1999). The sandy layer overlays a clay layer, which is situated at a depth of 0.7–2 m. As a result of the poor drainage, groundwater depth is typically high, fluctuating between 0.5 and 2 m (Carrara et al., 2003).

The pine stand was planted in 1929 (Neirynck et al., 2008). Until the autumn of 1999, when the forest was thinned, the tree density amounted to 542 trees ha⁻¹. The thinning decreased the tree density to 376 trees ha⁻¹. The average canopy height is 21.4 m (Op de Beeck et al., 2010). With a peak in leaf area index (LAI) of $1.3 \pm 0.5 \text{ m}^2 \text{ m}^{-2}$ in 2007 (Op de Beeck et al., 2010) and an average LAI of $1.2 \pm 0.5 \text{ m}^2 \text{ m}^{-2}$ in the period 1998–2007, the stand canopy is very sparse. Only two needle-age classes are present: current-year needles and 1-year-old needles (Op de Beeck et al., 2010).

The stand is part of the ICP Forests Level II and the Fluxnet CarboEurope-IP networks and is equipped with a 41 m tall instrumentation tower. Meteorological measurements and measurements of ecosystem CO₂ exchange with the eddy covariance technique have been conducted at the site on a continuous basis since 1996 (Gielen et al., 2013).

2.2 Measurements

The study covered the period 1998–2013, with the years 1999 and 2003 excluded due to poor data quality or coverage.

2.2.1 Meteorology

Air temperature (T_{air} ; °C) and humidity (RH; %) were measured with a PT100 and a HMP230 dew point transmitter (Vaisala, Helsinki, Finland) in aspirated radiation shields mounted on the tower at 2, 24, and 40 m of height. Wind speed (WS, m s⁻¹) was measured with a cup anemometer (LISA; Siggelkow GmbH, Hamburg, Germany) at 24, 32, and 40 m of height. Ingoing and outgoing shortwave and long-wave radiation were measured at the top of the tower with a CNR1 radiometer and a CMP6 pyranometer (Kipp and Zonen, Delft, The Netherlands). Rainfall was registered by a tipping bucket rain gauge (NINA precipitation pulse transmitter; Siggelkow GmbH, Hamburg, Germany). Both

T_{air} and RH were used to calculate the vapour pressure deficit (VPD; kPa). The soil temperature (T_{soil} ; °C) was measured at 9 cm below the soil surface with temperature probes (DPS-404; Oxsensis, Didcot, UK). The soil water content (SWC; $\text{m}^3 \text{ m}^{-3}$) was measured at 25 cm below the soil surface with time domain reflectometers (CS616; Campbell Scientific, Logan, Utah, USA). Instant SWC was read manually from the reflectometers every 3 to 14 days and values were interpolated to obtain daily estimates taking into account water inputs via precipitation (Gielen et al., 2010). The soil water potential (SWP; MPa) was derived from the SWC measurements with the model of van Genuchten (van Genuchten, 1980). All meteorological variables (except SWC and rainfall) were measured every 10 s and half-hourly means were calculated. Data gaps were filled with data from nearby weather stations.

2.2.2 Ozone mixing ratio

The O_3 mixing ratio ($[\text{O}_3]$; ppb) was measured at a 10 s resolution above the canopy at 24 m of height with a UV photometric analyzer (TEI 49i; Thermo Fisher Scientific, Waltham, MA, USA) and converted to half-hourly averages. Data gaps were filled with $[\text{O}_3]$ measurements done at 40 m of height. If these were not available, gaps were filled with $[\text{O}_3]$ measurements from a nearby weather station from the Flemish Environmental Agency (VMM) at Luchtbal, which is less than 10 km from the site.

2.2.3 Leaf area index

A continuous time series with daily LAI values was reconstructed for the pine stand based on the historical data. The general approach was to keep the seasonal pattern measured in 2009 by Op de Beeck et al. (2010) fixed for each year and to scale it year per year to the seasonal maximum LAI (LAI_{max}). LAI_{max} was measured with the LAI-2050 (LI-COR, Lincoln, Nebraska, USA) in 1997 and 2003 by Gond et al. (1999) and Konôpka et al. (2005), respectively, and with digital hemispherical photography in 2007 by Op de Beeck et al. (2010). To ensure consistency across the time series, the measurements were corrected for clumping using a factor of 0.83 (Jonckheere et al., 2005). The three measurements of LAI_{max} were interpolated linearly to derive LAI_{max} values for the missing years. The thinning event in 1999 was accounted for by subtracting the removed leaf biomass, determined with allometric relations from Yuste et al. (2005) and specific leaf area measurements from Op de Beeck et al. (2010).

2.2.4 Gross primary productivity

Gross primary productivity ($\mu\text{mol C m}^{-2} \text{ s}^{-1}$) was derived from net ecosystem exchange (NEE) measured with the eddy covariance technique and following the standard data quality procedures as explained in Appendix A. Half-hourly aver-

aged values of GPP were derived for the 14 growing seasons of the study period and integrated into daily and growing season totals.

2.2.5 Stomatal conductance

The measurements of stomatal conductance to H_2O ($g_{\text{st},\text{H}_2\text{O}}$) were done at needle level during the summers of 2007 (Op de Beeck et al., 2010) and 2013 to obtain data for the parameterisation of the multiplicative stomatal model used in the calculation of stomatal O_3 fluxes (see Sects. 2.3 and 2.4). The two summers were marked by quite different environmental conditions: cold and wet in 2007 and warm and dry in 2013. Measurements were carried out with the LI-6400 gas exchange system (LI-COR, Lincoln, Nebraska, USA) and included diurnal stomatal courses as well as stomatal responses to PAR, T_{air} , and VPD. Measurements were carried out on sets of three or four live fascicles, i.e. six to eight needles, which were enclosed in the LI-6400's leaf chamber while attached to the tree. Twenty-six needle sets were measured in total, equally divided between current-year and 1-year-old needles. Each needle set was harvested after being measured, and the hemi-surface needle area was determined in order to express $g_{\text{st},\text{H}_2\text{O}}$ on the correct needle area basis. Needle area was derived from needle dimensions (length and width at the top, middle, and base), assuming a hemi-circular cross-sectional needle area. The measurements of $g_{\text{st},\text{H}_2\text{O}}$ were converted to stomatal conductance to O_3 (g_{st}) by multiplying $g_{\text{st},\text{H}_2\text{O}}$ with the ratio of the molecular diffusivities of water vapour and O_3 (0.61).

2.3 Calculation of stomatal O_3 fluxes

The stomatal O_3 fluxes were calculated at a half-hourly resolution from a continuous series of half-hourly $[\text{O}_3]$ meteorology and daily LAI with an electric analogue model built from three resistances in series:

$$R_{\text{tot}} = R_{\text{aero}} + R_{\text{bl}} + R_{\text{can}}, \quad (1)$$

where R_{tot} is the total resistance to O_3 , R_{aero} is the aerodynamic resistance to O_3 , R_{bl} is the quasi-laminar boundary layer resistance to O_3 , and R_{can} is the canopy resistance to O_3 (all expressed in s m^{-1}).

The aerodynamic resistance was calculated following Grünhage (2002) with

$$R_{\text{aero}} = \frac{1}{\kappa u^*} \left[\ln \left(\frac{z-d}{z_0} \right) - \Psi_h \left(\frac{z-d}{L} \right) + \Psi_h \left(\frac{z_0}{L} \right) \right], \quad (2)$$

where κ is the von Karman constant (0.43), u^* (m s^{-1}) is the friction velocity, L is the Obukhov length, z is the $[\text{O}_3]$ measurement height (24 m), d is the zero plane displacement ($= 0.1 \text{ h}$), z_0 is the momentum roughness parameter ($= 0.65 \text{ h}$), h is the canopy height, and Ψ_h is the atmospheric stability function. This function is calculated using the set of coefficients published by Dyer (1974):

- for unstable atmospheric stratification ($L < 0$ m)

$$\Psi_h = 2 \cdot \ln \left[\frac{1}{\varphi_h(\zeta)} + 1 \right] \quad (3)$$

$$\varphi_h = (1 - 16 \cdot \zeta)^{-0.5} \quad (4)$$

$$\zeta = \frac{z - d}{L} \text{ with } z = z_2 = z_{\text{ref},T} \quad (5)$$

and $z = z_1 = d + z_0$; (5)

- for stable atmospheric stratification ($L > 0$ m)

$$\Psi_h = -5 \cdot \zeta \quad (6)$$

$$\zeta = \frac{z - d}{L} \text{ with } z = z_2 = z_{\text{ref},T} \quad (7)$$

and $z = z_1 = d + z_0$; (7)

- and for neutral atmospheric stratification ($|L| \rightarrow \infty$).

$$\Psi_h = 0 \quad (8)$$

The quasi-laminar boundary layer resistance was calculated following Baldocchi et al. (1987) with

$$R_{\text{bl}} = \frac{2}{\kappa \cdot u^*} \left(\frac{Sc}{Pr} \right)^{2/3}, \quad (9)$$

where κ is the von Karman constant (0.43), u^* (m s^{-1}) is the friction velocity, which is derived from the measured momentum fluxes, Sc is the Schmidt number (1.07 for O_3), and Pr is the Prandtl number (0.72 for O_3).

The canopy resistance was calculated from a stomatal resistance (R_{st}) and a non-stomatal resistance (R_{nst}) mounted in parallel:

$$R_{\text{can}} = \left(\frac{1}{R_{\text{st}}} + \frac{1}{R_{\text{nst}}} \right)^{-1}. \quad (10)$$

The stomatal resistance R_{st} was calculated with an algorithm that divides the pine canopy into eight horizontal leaf layers, with the LAI being divided equally between the layers, that simulates the transfer of radiation through the layered canopy. The algorithm then calculates the stomatal resistance for the sunlit and shaded area fraction of each leaf layer with the multiplicative stomatal model described by Jarvis (1976) and reformulated by Emberson et al. (2000). Resistance values are then integrated over all layers to obtain canopy level R_{st} . The algorithm is explained in more detail in Op de Beeck et al. (2010). The version of the multiplicative stomatal model used in this study is described in detail in Appendix B. This model was given a site-specific parameterisation as explained in Sect. 2.4.

The non-stomatal resistance R_{nst} was assumed to be constant in time and set to 279 s m^{-1} . This value was derived from the long-term O_3 flux measurements in Brasschaat (Neirynck et al., 2012).

Total and stomatal O_3 fluxes (F_{tot} and F_{st} ; $\text{nmol m}^{-2} \text{s}^{-1}$) were calculated on a half-hourly basis with

$$F_{\text{tot}} = 44.64 \frac{[\text{O}_3]}{R_{\text{tot}}} \quad (11)$$

$$F_{\text{st}} = F_{\text{tot}} \frac{R_{\text{can}}}{R_{\text{st}}}, \quad (12)$$

where 44.64 is the molar density of air in mol m^{-3} at an air pressure of 101.3 kPa and an air temperature of 0°C , used here to convert flux units from m s^{-1} to $\text{mol m}^{-2} \text{s}^{-1}$. Half-hourly fluxes were aggregated to daily and yearly values.

2.4 Parameterisation and validation of the multiplicative stomatal model

The multiplicative stomatal model was parameterised and validated against the dataset of g_{st} measurements collected at the site. This dataset included, in addition to the measured g_{st} , also PAR, T_{air} , VPD, and SWP and was split into a parameterisation set and a validation set by grouping the odd and even rows of data after being ranked by PAR. The parameterisation was done by optimising the model parameters with the function “lsqcurvefit” in Matlab (Matlab, Natick, MA, USA; Statistics Toolbox Release, 2013a), which finds the best parameter values starting from an initial value and which can be used to fit non-linear functions with more than two independent variables. The parameters of the boundary functions f_{PAR} , $f_{T_{\text{air}}}$, f_{VPD} , and f_{SWP} were optimised separately, starting from initial values that were estimated visually from plots of g_{st} versus each of the input variables (PAR, T_{air} , VPD, and SWP). The phenology function f_{phen} was set to 1 for the parameterisation of f_{PAR} , $f_{T_{\text{air}}}$, f_{VPD} , and f_{SWP} since g_{st} had been measured on mature needles only. We included f_{phen} in the final model to estimate the stomatal O_3 fluxes over the growing season (Appendix B).

The parameterised model was then tested against the validation dataset. The model performance was evaluated with the linear regression $y = ax + b$ fitted to the plot of the measured versus the modelled g_{st} and with the following set of performance statistics: the coefficient of determination (R^2), mean bias (MB), relative mean error (RME), Willmott's index of agreement (d), model efficiency (ME), and root mean square error (RMSE) and its systematic (RMSE_s) and unsystematic (RMSE_u) components. These statistics are explained briefly in Appendix C. To visually evaluate the goodness-of-fit of each boundary function, the modelled g_{st} was plotted versus each of the input variables and the corresponding boundary function added to the scatter plot.

2.5 Detecting O_3 effects on GPP

We adopted a modelling approach to detect possible O_3 effects on GPP. Under the assumption that O_3 -induced GPP reduction is most likely to occur during and shortly after days of high stomatal O_3 fluxes, we parameterised a GPP model

against a dataset from which such days were removed and then we simulated the daily and growing season GPP with this supposedly O₃-damage-free model. A reduction in GPP due to O₃ would become apparent as a model overestimation of daily GPP for the days on which an O₃ effect was assumed, and possibly also as an overestimation of growing season GPP. The physiological mechanism beyond the assumption made above is that at high stomatal O₃ fluxes, the trees' defensive mechanisms cannot detoxify all O₃ entering the needles and damage is caused to the photosynthetic apparatus (Dizengremel, 2001; Matyssek and Sandermann, 2003). This leads to decreased gross photosynthetic rates and GPP. The damage is repaired afterwards when the stomatal O₃ load decreases.

We used a feed-forward back propagation artificial neural network (ANN) as a GPP model in Matlab (Matlab, Natick, MA, USA). The ANN contained 10 nodes organised in 1 layer, which came out as the best performing network after comparing networks containing different numbers of nodes and/or layers (data not shown). The default settings of the Matlab Neural Network Toolbox were used. A normalisation process was applied for training and testing the data; data were scaled to [-1 1] based on the lowest and highest value in the dataset. We used the Levenberg–Marquardt algorithm to train the ANN for 1000 iterations (Marquardt, 1963). The progress of the training procedure was monitored using the mean square error (MSE) of the network. The daily GPP data were used as dependent target variables in the ANN. The input variables were year, day of the year, T_{\min} , T_{\max} , T_{mean} , average VPD, SWC, R_g , average T_{soil} , and average WS. The daily totals of the variables were used, with the exception of VPD, T_{soil} , and WS, for which the daily averaged values were used. The individual weights of these parameters on our model were estimated by replacing each input variable with a random permutation of its values. This was done for the GPP model, as described above, and a GPP model containing O₃ as an input variable to test whether O₃ had any explanatory power on GPP.

To obtain an O₃-damage-free GPP model, the days for which an O₃ effect on GPP was expected were removed from the dataset. We assumed that if an O₃ effect occurs, it would occur on the days with the highest stomatal O₃ fluxes. Because the defensive capacity of the pine trees was not quantified, and hence the O₃ load above which O₃ would affect GPP was not known, we repeated the analysis twice by removing the days with the 2, 5, and 10 % highest stomatal O₃ fluxes. Because the results for a 2 and 10 % cut-off were equal to those for a 5 % cut-off, we report only the results for a 5 % cut-off. The model was trained with two-thirds of the remaining dataset, while the other one-third was used to test the model. This O₃-damage-free model was then run with the full dataset.

The model overestimation of daily GPP was evaluated (1) from the linear regression on the data of the measured versus the modelled GPP for the days on which an O₃ effect

was assumed, testing whether the regression slope and intercept were different from 1 and 0, respectively, and (2) by comparing the measured and the modelled daily GPP for these days by means of a paired-samples *t* test or a Wilcoxon signed-rank test if differences were not normally distributed (Shapiro–Wilk test). A significant outcome of this test in combination with a regression slope significantly lower than 1 (and an intercept not different from 0) would together point to a significant overestimation of GPP. Furthermore, (3) the regression slope and intercept were compared with the slope and intercept of the regression fitted to the dataset used to train and test the GPP model. This was done to evaluate whether GPP estimations for the days on which we assumed an O₃ effect were, in relative terms, significantly higher than GPP estimations for the days used for model training and testing. This would become apparent as a significantly lower slope (with an intercept no different from 0). The model overestimation of the growing season GPP was evaluated with the first two tests above on the growing season data. Additionally, the residuals of growing season GPP (model – measurement) were plotted against AOT40, POD₁, and total growing season stomatal O₃ uptake and linear regression lines were fitted. It was tested whether the regression slope and intercept were significantly different from 0 to assess the presence of a statistically significant O₃ dose–response relationship.

Since it may take some time for trees to repair the damage to the photosynthetic apparatus induced by O₃, O₃ effects might last several days after a peak of O₃ exposure. They might thus not be detected with the model parameterised as explained above. To account for such a sustained O₃ effect, the modelling was repeated, now not only excluding the days with the highest stomatal O₃ fluxes from the dataset for model training but also the following days. The modelling was repeated with three different such delay periods: the first, the first 2, and the first 6 days following each flux peak. The results were evaluated with the same statistical tests as mentioned above. Because the results were similar for the three delay periods, only the results for the 2-day period are shown.

High O₃ events are often coupled with specific meteorological conditions, i.e. high radiation and air temperatures. Since the dataset for the model training had been compiled by removing the days with the highest stomatal O₃ fluxes, it was not unlikely that these conditions were underrepresented in the training dataset. If so, this could induce a bias in the model response to radiation and temperature and possibly result in overestimations of GPP for the days on which an O₃ effect was expected, which we then might wrongly attribute to O₃. To evaluate the risk for such model bias, we compared the frequency distribution, range of radiation, T_{\min} , T_{\max} , T_{mean} , and VPD between the training dataset and the dataset with the days on which we expected an O₃ effect.

One of the assumptions in our approach is that the O₃ effects on GPP are short term, i.e. they last just a few days, and are hence not carried over. The presence of a carry-over effect would compromise the validity of our approach. We

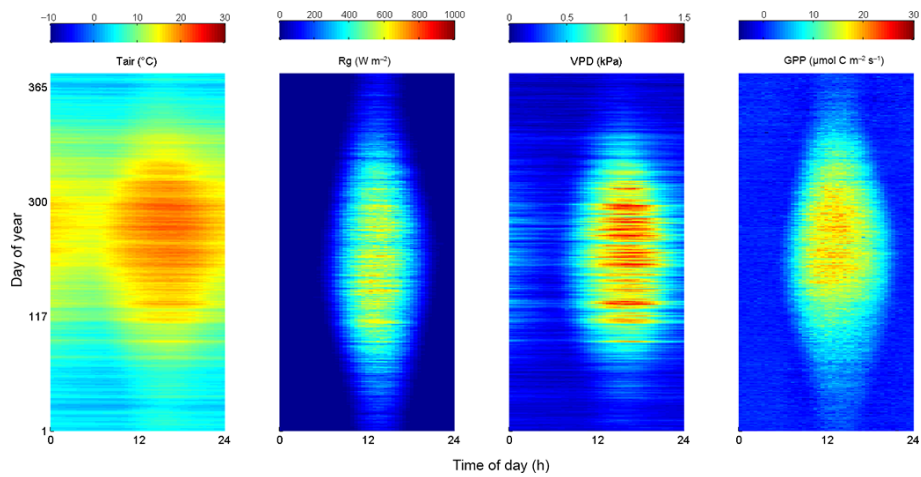


Figure 1. The fingerprint of air temperature (T_{air}), incoming global radiation (R_g), vapour pressure deficit (VPD), and measured gross primary productivity (GPP) averaged over the period 1998–2013. The day of the year is plotted on the y axis and the hour of the day on the x axis.

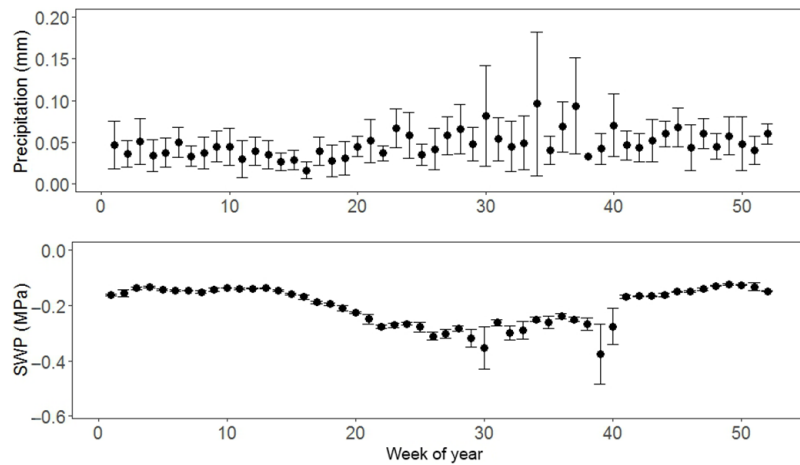


Figure 2. The time series of the weekly total precipitation and mean soil water potential (SWP). The precipitation and SWP data are averaged over the period 1998–2013. The error bars represent the 95 % confidence intervals.

can rule out a carry-over effect by testing whether trees exposed to low stomatal O₃ fluxes late in the growing season behave in the same way as when exposed to similarly low O₃ fluxes early in the growing season. To test this, we compiled a dataset that contained only the days after the first major peak of stomatal O₃ flux in the growing season. From this period, we further selected only the days with low stomatal O₃ fluxes for which no short-term O₃ effect was expected. In other words, we excluded the days with a peak of stomatal O₃ flux plus the 6 following days. We trained the GPP model with these data and then predicted GPP for the days before the first major O₃ peak in each growing season. If a carry-over effect was present, or at least an effect induced during the first major O₃ flux peak, it would be somehow included in the trained model. This would then underestimate GPP for the days before each first major O₃ peak, where a carry-over

effect has assumptively not yet occurred. The model underestimation of GPP was evaluated from a linear regression on the data of the measured versus the modelled GPP, testing whether the regression slope and intercept were different from 1 and 0, respectively. This slope and this intercept were also compared with the slope and intercept of the regression line fitted to the training data. Also, the measured and modelled GPP were compared with a paired-samples *t* test or a Wilcoxon signed-rank test whether differences were not normally distributed (Shapiro–Wilk test).

All statistics were performed with R version 3.2.3 (The R Project for Statistical Computing Core Team, Vienna, Austria 2015) at a significance level of $p = 0.05$.

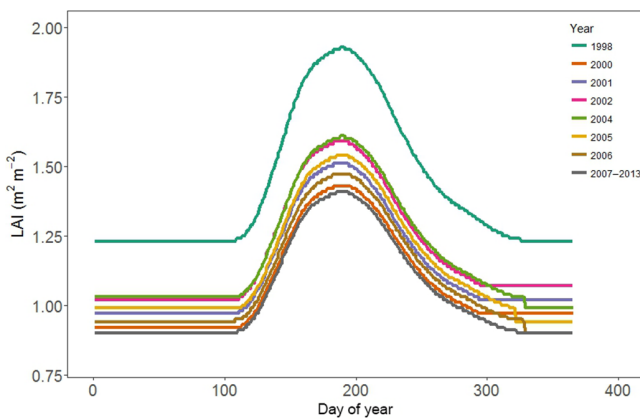


Figure 3. The seasonal course of the LAI for each of the 14 growing seasons used in this study.

3 Results

3.1 Measurements: meteorology, GPP, and LAI

Figure 1 shows a fingerprint of the multi-annual average diel and seasonal patterns of the main meteorological variables T_{air} , incoming global radiation (R_g), and VPD as well as measured GPP. This figure gives a good overview of how meteorology and GPP typically changed over time in this forest; inter-annual anomalies from the average patterns can be found in Fig. S1 in the Supplement. Distinct daily and seasonal patterns can be observed; for example, reaching the highest values in summer in the afternoon. Similar patterns can also be observed in GPP, which basically follows the pattern of R_g . As seen in Fig. 1, the photosynthetic period extends, on average, from day of the year 115 (the end of April) till day of the year 300 (the end of October). The time series of precipitation and SWP are provided in Fig. 2, while the seasonal LAI courses are shown for each year in Fig. 3. The yearly maximum LAI ranged from 1.4 to 1.9 $\text{m}^2 \text{m}^{-2}$. The thinning of the forest in 1999 can clearly be observed in the LAI pattern. After the thinning, the canopy never fully closed.

3.2 Multiplicative stomatal model and simulated O₃ fluxes

The optimised parameter values of the model are presented in Table 1. The different statistics to evaluate the model performance are presented in Table 2, and this is for both the parameterisation and the validation dataset. For the parameterisation dataset, the measured data were plotted against modelled g_{st} and plotted in Fig. 4a. The slope of the linear fit was not significantly different from 1 ($p = 0.87$) and the intercept was not significantly different from 0 ($p = 0.81$). The model evaluation for the validation dataset was equally good as for the parameterisation dataset (Table 2). Also, in the linear fit for the validation set (Fig. 4, b), the slope was

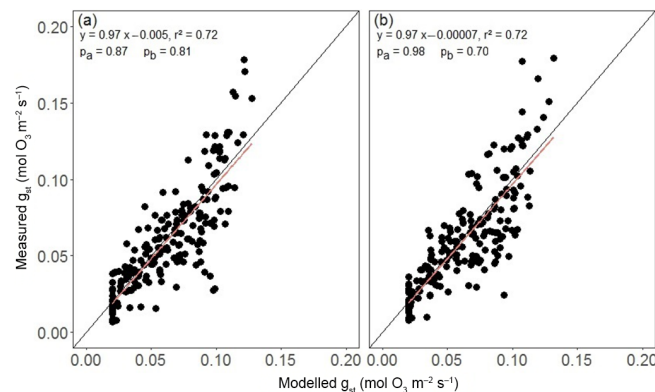


Figure 4. The measured versus the modelled stomatal conductance (g_{st}) for the parameterisation dataset (a) ($n = 205$) and the validation dataset (b) ($n = 205$). The black line is the 1:1 line. The red line is the linear fit for which the equation is given in the figure. Also shown are the p values of the tests for the slope being different from 1 (p_a) and the intercept different from 0 (p_b).

Table 1. The optimised parameter values of the multiplicative stomatal model.

$g_{\text{max}} (\text{mol O}_3 \text{ m}^{-2} \text{ s}^{-1})$	0.14
$g_{\text{min}} (\text{mol O}_3 \text{ m}^{-2} \text{ s}^{-1})$	0.02
a_{PAR}	0.0057
$T_{\text{opt}} (\text{°C})$	25.61
$T_{\text{min}} (\text{°C})$	5.47
$\text{VPD}_{\text{min}} (\text{kPa})$	3.16
$\text{VPD}_{\text{max}} (\text{kPa})$	0.51
$\text{SWP}_{\text{min}} (\text{MPa})$	-1.18
$\text{SWP}_{\text{max}} (\text{MPa})$	-0.19

not significantly different from 1 ($p = 0.98$) and the intercept was not significantly different from 0 ($p = 0.70$).

Figure 5 shows the scatter plots of the measured g_{st} versus each of the model input variables PAR, T_{air} , VPD, and SWP and the fitted boundary function for each plot.

The average daily O_3 fluxes for the different years are presented in Fig. S2. Daily F_{st} ranges from 1.12 to 1.52 $\text{nmol O}_3 \text{ m}^{-2} \text{ day}^{-1}$. In 2011, the daily F_{st} was the lowest, while the highest values were observed in 2002. The annual average ratio $F_{\text{st}}/F_{\text{tot}}$ varied between 24 and 28 % (Fig. S2). We observed the lowest ratios at the beginning and at the end of the growing season. Above-average ratios were observed at the peak of the growing season.

3.3 Ozone effects on GPP

Figure 6 shows the frequency distributions of R_g , T_{min} , T_{max} , T_{mean} , and VPD for the training dataset and the dataset with days on which we assumed an O_3 effect. Days in the latter dataset are generally more concentrated in the upper half of each variable's range. The training dataset includes more days in the lower half, but conditions of high radiation, tem-

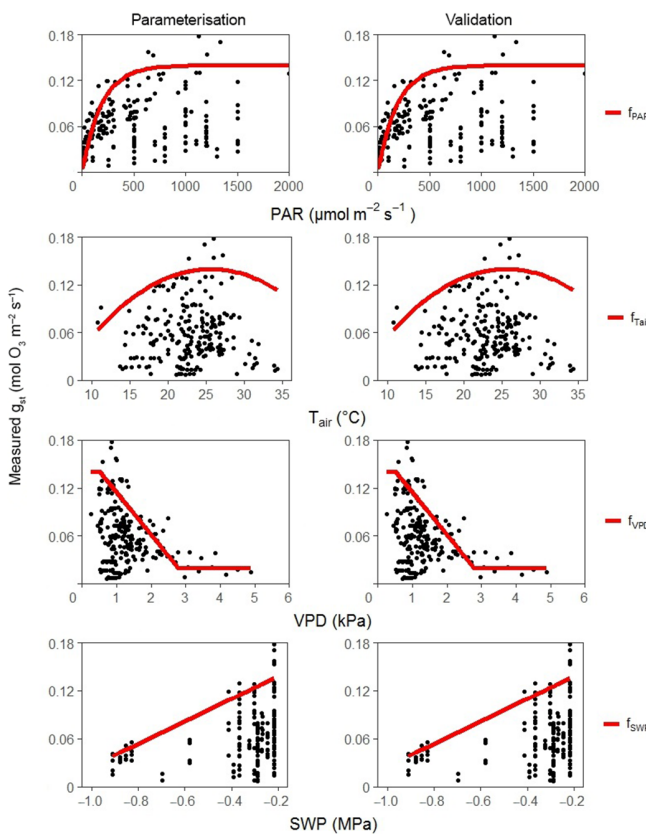


Figure 5. The measured stomatal conductance (g_{st}) as a function of the different variables used in the multiplicative model: photosynthetically active radiation (PAR), air temperature (T_{air}), vapour pressure deficit (VPD), and soil water potential (SWP). The red line represents the boundary line for which the functions are given in Appendix B (Eqs. B3–B6) ($n = 205$).

perature, or VPD do not seem to be underrepresented as the dataset also included a substantial number of days in the higher part. For all variables, the variable range of the dataset with days for which we assumed an O₃ effect is a fully contained range of the training dataset.

All parameters in the GPP model were ranked according to their contribution to GPP prediction (Table 3). Global radiation is the most important parameter in defining GPP, with a mean square error (MSE) of 37 500.81 mol m⁻² s⁻¹, followed by day of the year (30 240.61 mol m⁻² s⁻¹) and year (27 486.63 mol m⁻² s⁻¹). The maximum air temperature and VPD contribute equally to the model with an MSE of about 15 300 mol m⁻² s⁻¹. Wind velocity, T_{min} , and SWC contribute the least to GPP. Ozone as an input variable had an MSE of 11 885.73 mol m⁻² s⁻¹ (Table 3b) and contributed the least with an MSE similar to the overall model (10 019.30 mol m⁻² s⁻¹).

To test for carry-over O₃ effects, we evaluated and compared the linear regressions of the measured versus the modelled GPP of a dataset with low O₃ fluxes after the first ma-

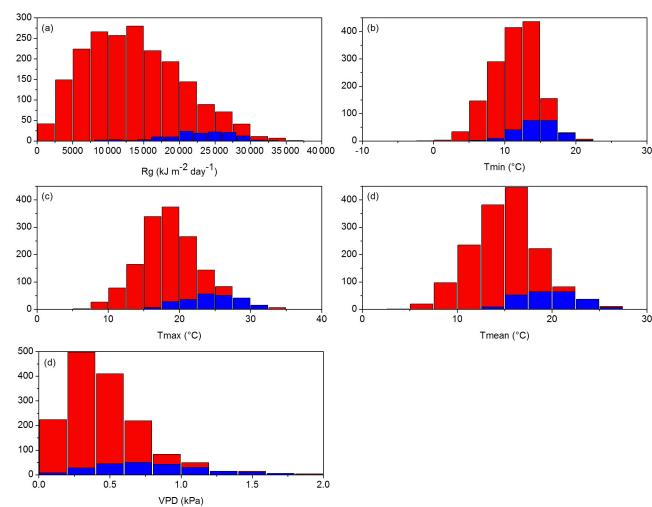


Figure 6. Histograms of the meteorological variables for the training dataset (red) and the high O₃ uptake dataset (blue). The subplots represent global radiation R_g (a), minimum temperature T_{min} (b), maximum temperature T_{max} (c), mean temperature T_{mean} (d), and vapour pressure deficit VPD (e).

Table 2. Performance statistics for the multiplicative stomatal model: mean bias (MB), relative mean error (RME), systematic and unsystematic root mean square error (RMSE_{s/u}), Willmott's index of agreement (d), model efficiency (ME), and the coefficient of determination (R^2).

Statistics	Parameterisation	Validation
MB	0.002	0.002
RME	0.34	0.33
RMSE	0.019	0.019
RMSE _s	0.006	0.006
RMSE _u	0.017	0.017
d	0.99	0.99
ME	0.72	0.72
R^2	0.72	0.72

jor O₃ flux peak in the growing season and a dataset before this peak (Fig. 7). For both regressions, the intercept and slope were not significantly different from 0 and 1 respectively (training: $p_{slope} = 1$, $p_{intercept} = 1$; testing: $p_{slope} = 0.83$, $p_{intercept} = 0.44$). The slopes were also not significantly different from each other ($p = 0.86$), and neither were the intercepts ($p = 0.53$).

Figure 8 shows the measured versus the modelled daily GPP for the model trained without the days with the highest stomatal O₃ fluxes (GPP model 1) and the model trained to also test for lag effects (GPP model 2). Both models reproduced daily GPP well for the dataset against which they were trained and tested, as indicated by the high R^2 values and the fitted regression lines falling on the 1:1 line (Fig. 8a, b). For both models, the regression slope for the

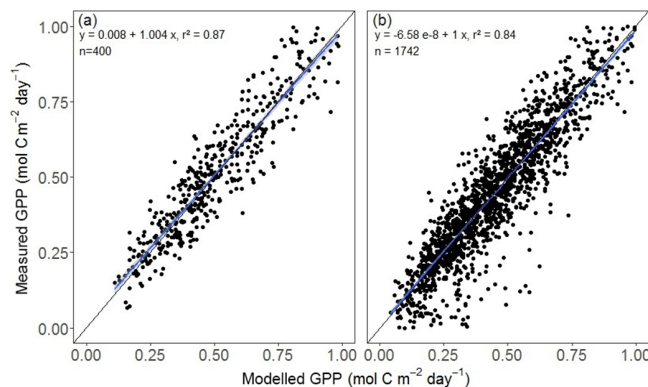


Figure 7. The measured GPP plotted as a function of the modelled GPP for two different datasets: **(a)** only the days before the first major O₃ peak in every year and **(b)** the training dataset with the days after the first major O₃ peak in every year, excluding those with high O₃ fluxes plus 6 following days to train the network. The black line is the 1 : 1 line. The blue line is the regression fit including 95 % confidence intervals (in grey).

dataset with the days on which we assumed an O₃ effect was significantly lower than 1 and the intercept significantly higher than 0 (Fig. 8c, d). For GPP model 1, the regression slopes were not significantly different between the two datasets ($p = 0.46$), but the intercepts were ($p < 0.05$). For GPP model 2, both the regression slopes and intercepts differed significantly ($p < 0.001$ and $p < 0.001$). However, a Wilcoxon signed-rank test showed for both models that the modelled daily GPP was not significantly higher than the measured daily GPP for the days on which an O₃ effect was assumed ($p = 0.83$ and $p = 0.64$, respectively). Also, a paired-samples *t* test showed for both models that the modelled growing season GPP was not significantly higher than the measured growing season GPP ($p = 0.93$ and $p = 0.55$, respectively). The slope and intercept of the linear regression line were not significantly different from 1 and 0 (Fig. 8e, f).

No statistically significant correlations were found between the model residuals of growing season GPP and total stomatal O₃ uptake (F_{st}), AOT40, and POD₁ (Fig. 9). Figure S4 shows the relation between the measured growing season GPP, F_{st} , AOT40, and POD₁, as well as the time series of these parameters. No statistically significant correlations were found between the measured growing season GPP and AOT40 and POD₁. A significantly negative correlation was found between the measured growing season GPP and F_{st} ($p = 0.006$) due to a decline in GPP at a low F_{st} ($F_{st} < 70 \text{ mmol O}_3 \text{ m}^{-2}$).

Table 3. The ranking of the parameters defining GPP in the ANN by replacing each input variable with a random permutation of its values. **(a)** The parameters with their mean square error (MSE; mol m⁻² day⁻¹) for the model without O₃. **(b)** The parameters with their MSE for the model with O₃. The overall model MSE without any random permutation is also shown.

Ranking No.	(a)	(b)
1	$R_g - 37\ 500.81$	$R_g - 41\ 358.93$
2	doy – 30 240.61	year – 33 978.09
3	year – 27 486.63	doy – 31 127.90
4	VPD – 15 380.68	$T_{soil} - 24\ 893.78$
5	$T_{max} - 15\ 323.22$	$T_{max} - 23\ 567.45$
6	$T_{soil} - 15\ 076.75$	$T_{mean} - 21\ 354.76$
7	$T_{mean} - 13\ 858.91$	VPD – 16 395.14
8	WV – 13 369.01	$T_{min} - 15\ 418.16$
9	$T_{min} - 12\ 732.96$	WV – 14 685.97
10	SWC – 12 402.04	SWC – 12 831.19
11		O ₃ – 11 885.73
Overall model MSE	11 360.85	10 019.30

4 Discussion

4.1 Multiplicative stomatal model

All statistics shown in Table 2 clearly indicated that the fitted multiplicative stomatal model performed well. For both the parameterisation and the validation datasets, the model explained 72 % of the variance in g_{st} . For both datasets, the slope and intercept of the linear regression lines of the measured versus the modelled g_{st} were not significantly different from 1 and 0, respectively (Fig. 4). Moreover, the model efficiency (ME in Table 2) of 0.72 and the Wilmott's index (*d*) close to 1 both indicate that the modelled values matched the measured values well. A good model provides low root mean square error (RMSE), while the systematic component (RMSE_s) should approach zero and the unsystematic component (RMSE_u) should approach the RMSE (Willmott et al., 1985), which was the case for this model. A low mean bias (MB) and a low mean relative error (MRE) further indicated a very good performance. The good performance of the model can also be observed in Fig. 5, in which the boundary lines represent the response of g_{st} to the independent variables when other variables were not limiting. The boundary lines fitted close to the data points, which is an indication of a good model because the multiplicative stomatal model is based on the assumption that the variables act more or less multiplicatively and independently from each other (Grüters et al., 1995).

As explained in the mapping manual of the Convention on Long-Range Transboundary Air Pollution (CLRTAP), Scots pine is the representative species to assess the risk of O₃ damage to coniferous forests in Atlantic central Europe (CLRTAP, 2015). This risk is assessed on the basis of O₃

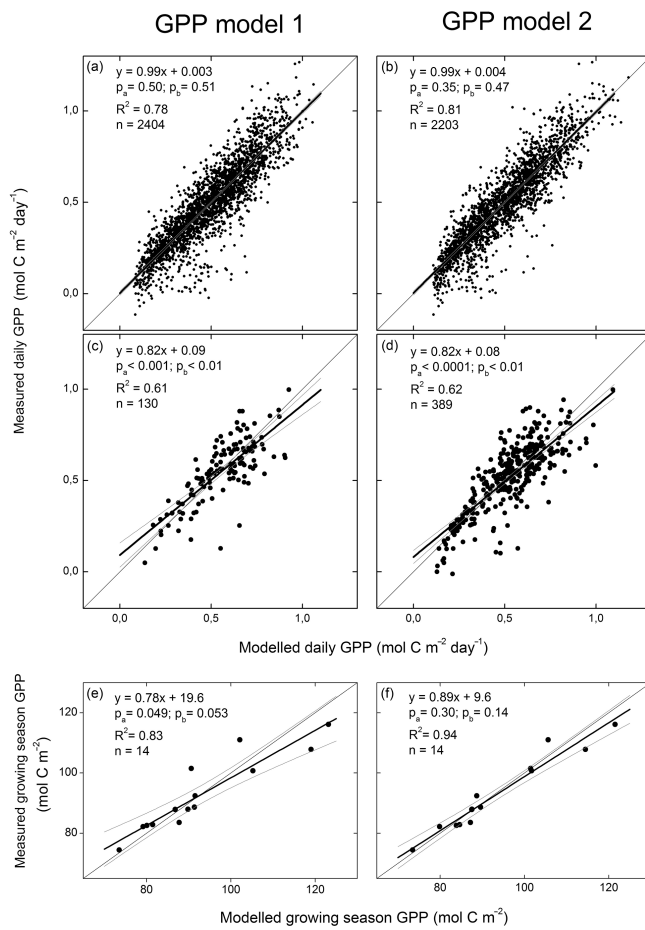


Figure 8. The measured versus the modelled gross primary productivity (GPP) for days used for model training and testing (**a, b**), for days on which an O₃ effect was assumed (**c, d**), and for the entire growing season (**e, f**). GPP model 1 was trained without days with the highest stomatal O₃ uptake, whereas GPP model 2 was trained to test for possible lag effects of O₃ on GPP. The black lines are the fitted linear regression lines and the grey lines mark the 95 % confidence bands. Also shown are the *p* values for the tests of the slope and intercept from the regression $y = ax + b$ being different from 1 and 0, respectively.

doses calculated with the DO₃SE algorithm, which employs a Jarvis-type stomatal model that has been parameterised for Scots pine based on a compilation of primary and secondary data (Emberson et al., 2007; Büker et al., 2015; CLRTAP, 2015). The parameterisation for our Scots pine stand differs in some numbers from the one used in the DO₃SE algorithm. The most remarkable difference is that the g_{\max} of the Scots pines in Brasschaat is much lower (0.14 vs. 0.18 mol O₃ m⁻² s⁻¹). This low g_{\max} may imply that, during episodes of high O₃ mixing ratio, the Brasschaat site is unlikely to take up very high amounts of O₃ (Altimir et al., 2004; Emberson et al., 2007). This may have contributed to the absence of a clear O₃ response at our site. A second difference is that the stomata of the pine trees re-

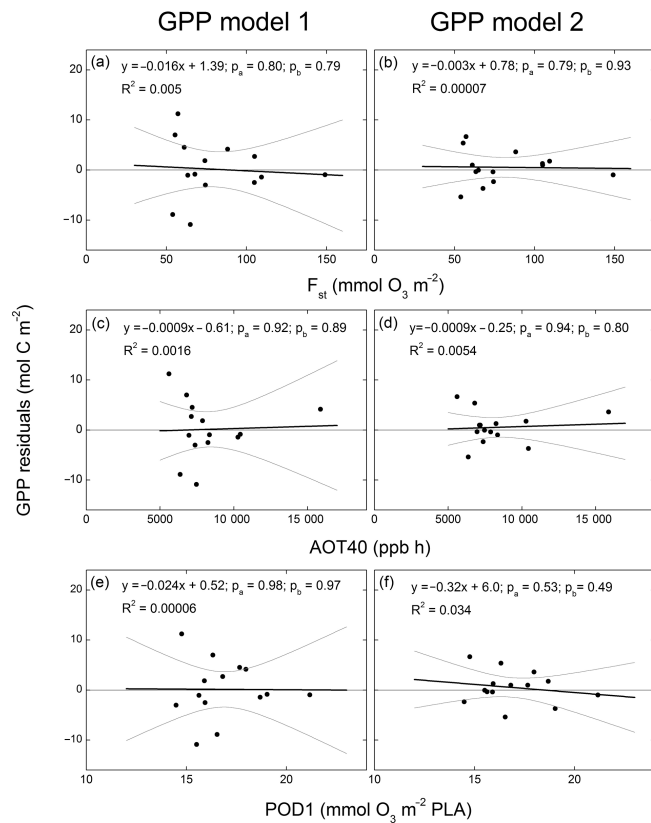


Figure 9. The residuals of growing season gross primary productivity (GPP) as a function of (**a, b**) the total stomatal O₃ flux over the growing season (F_{st}), (**c, d**) AOT40, and (**e, f**) POD₁. PLA is the projected leaf area. The negative residuals indicate model overestimation of GPP. GPP model 1 was trained without days with the highest stomatal O₃ uptake, whereas GPP model 2 was trained to test for possible lag effects of O₃ on GPP. The black lines are the fitted linear regression lines and the grey lines mark the 95 % confidence bands. Also shown are the *p* values for the tests of the slope and intercept from the regression $y = ax + b$ being different from 0 ($n = 14$).

main opened at night ($g_{\min} = 0.02 \text{ mol O}_3 \text{ m}^{-2} \text{ s}^{-1}$), while the DO₃SE model simulates full stomatal closure. Furthermore, the response to temperature for our Scots pine stand is shifted slightly higher ($T_{\text{opt}} = 25$ vs. 20 °C) and the response to soil drought is much stronger (SWC_{max} = −0.19 vs. −0.7 MPa and SWC_{min} = −1.18 vs. −1.5 MPa). From these differences, it can be inferred that stomatal O₃ uptake rates at the Brasschaat site are considerably lower than would be simulated with the DO₃SE model for generic Scots pine. This highlights the importance of a site-specific parameterisation when aiming to assess stomatal O₃ loads at site level.

4.2 Stomatal O₃ fluxes

The stomatal O₃ flux contributed on average 26 % to the total O₃ flux over the study period (Fig. S2). This fraction is similar to the 21 % stomatal O₃ flux in a Danish Norway spruce stand (Mikkelsen et al., 2004) and the 30 % stomatal O₃ flux in *Quercus ilex* in Italy (Vitale et al., 2005; Gerosa et al., 2005). Cieslik (2004) showed that in southern Europe, the stomatal O₃ flux of different vegetation types, such as pine forests and Mediterranean shrubs, is typically less than 50 % of the total O₃ flux. A 5-year study on a Mediterranean *Pinus ponderosa* stand showed a stomatal O₃ flux contribution of 57 % (Fares et al., 2010). Clearly, species- and site-specific differences, such as tree age or micro-climate, are introducing large variability in stomatal O₃ uptake (Neirynck et al., 2012).

The low relative stomatal O₃ flux in the Scots pine stand in Brasschaat could be the result of the sparse canopy with low LAI. Although no relation between stomatal O₃ flux and LAI was found in a previous study on this site (Neirynck et al., 2012), inter-annual and seasonal variation in LAI is very small, rendering such a correlation analysis very difficult.

4.3 Ozone effects on GPP

A comparison of the frequency distributions of radiation, temperature, and VPD between the training dataset and the dataset with the days on which we expected an O₃ effect showed that the meteorological conditions in the latter dataset were fully represented in the training dataset. From the full overlap, we can rather safely assume that the GPP model did not include a biased response to these variables that could result in a GPP overestimation that we might wrongly interpret as an effect of O₃. Also, O₃ as an input variable in the ANN did not have any explanatory power on GPP as it had the lowest MSE value close to the overall model MSE. Furthermore, a GPP model parameterised to include a carry-over effect of O₃ on GPP did not overestimate GPP at a statistically detectable level for days on which such an effect was not assumed to occur. From these results, we infer that carry-over effects of O₃ were unlikely to have occurred and that the assumption of the absence of (detectable) carry-over effects was valid.

The statistical tests on the datasets of the measured and the modelled GPP did not reveal a statistically significant model overestimation of daily GPP for the days on which we assumed an O₃ effect nor an overestimation of growing season GPP. Also, no significant correlations were found between growing season GPP residuals and stomatal O₃ flux, AOT40, and POD₁, even though critical levels for AOT40 and POD₁ were exceeded in every single year of our study period. From these results and within the limits of the modelling approach applied in this study, we can infer that no significant effect of O₃ on GPP occurred.

Some earlier studies have investigated the effect of O₃ on forest carbon uptake. A cumulative stomatal uptake of 27 mmol m⁻² over the growing season did not result in any visible damage or a reduction in NEE on a poplar plantation in Belgium (Zona et al., 2014). Zapletal et al. (2011), on the other hand, reported that the CO₂ uptake of a Norway spruce forest in the Czech Republic increased with increasing stomatal O₃ flux followed by a sudden decrease in CO₂ uptake, suggesting that an O₃ flux threshold exists. Fares et al. (2013) showed a negative correlation between GPP and O₃ uptake in two Mediterranean ecosystems (a forest dominated by *Pinus ponderosa* and an orchard of cultivated *Citrus sinensis*, both in California, USA). A GPP reduction of 1–16 % in response to O₃ uptake under an ambient O₃ mixing ratio of 30–50 ppb was determined across vegetation types and environmental conditions in the United States by Yue and Unger (2014). The magnitude of the reduction depended on the sensitivity to O₃ of the species and on the biome types.

AOT40 is, at present, the European standard for forest protection (EEA, 2014) with a critical level of 5000 ppb h, equivalent to a growth reduction of 5 % (CLRTAP, 2015). In this study on Scots pine in Brasschaat, this value was far exceeded in all years (Fig. 9), yet no negative effect on GPP was observed in years with higher AOT40 values.

POD₁ is considered a more appropriate index for potential O₃ damage because it considers O₃ flux. The critical level of POD₁ is species-specific; a critical level of 8 mmol m⁻² with a 2 % growth reduction is used for Norway spruce and a critical level of 4 mmol m⁻² with a 4 % growth reduction is used for birch and beech (CLRTAP, 2015). A critical level for Scots pine has not yet been determined, and therefore the value of 8 mmol m⁻² for Norway spruce is often adopted as a critical level for Scots pine. During our 14-year study period, this critical level was exceeded every single year, and again no significantly negative correlation between total GPP residuals and POD₁ was observed. In comparison to the AOT40 level, 2006 was not the year with the highest POD₁. This difference between AOT40 and POD₁ in 2006 was due to stomatal closure; during high O₃ mixing ratio events, *g_{st}* was rather low (Fig. S3). POD₁ was highest in the year 2002, when O₃ mixing ratios were relatively low, but *g_{st}* was high. The low O₃ mixing ratios explain the lower AOT40 for 2002.

Notwithstanding the absence of a statistically significant positive correlation between GPP residuals and both AOT40 and POD₁, critical levels for both AOT40 and POD₁ were exceeded every single year. AOT40 is based on O₃ mixing ratios, and these concentration-based indices have been shown to be weaker indicators of O₃ damage than flux-based indices (Karlsson et al., 2007; Simpson et al., 2007). The critical level of POD₁ for Scots pine was adopted from the critical level for Norway spruce (CLRTAP, 2015). Possibly, this critical level is too low for Scots pine.

Figure S4 shows a negative relationship between the measured growing season GPP and the O₃ dose, most notably and only significant between GPP and *F_{st}* (Fig. S4a). These

trends suggest a strong effect of O₃ on GPP, which contradicts the outcome of our modelling analysis. The relationships are negative because the steady GPP increase that can be observed from the year 2005 until the end of the study period coincides with a steady decrease in O₃ loads (Fig. S4d, e, f). To our judgement, this GPP increase is more likely to be the result of forest regrowth in response to decreased acidification at the site (Neirynck et al., 2008) than a response to decreased O₃ loads. This forest regrowth is accounted for in our modelling analyses by means of the LAI input in the ANN, allowing us to disentangle the effect of both factors on GPP. We furthermore believe that the observed trends do not reflect a causal relationship between GPP reduction and O₃ loads because the GPP decrease is the strongest at low O₃ loads but virtually absent at high O₃ loads (Fig. S4a, b). This is not what would be expected in the case of an O₃ effect.

Overall, no significant O₃ effects on daily and growing season GPP were found with our modelling approach. It can thus be concluded that O₃ did not affect the GPP of the pine forest, at least not if the assumptions we made in our approach to detect O₃ effects are valid. The most crucial assumption involves the distinction between days at which a GPP effect did and did not occur. It was not possible to identify these days with great precision due to lack of knowledge on the defensive capacity of the trees and their ability to repair O₃ damage. To overcome this, we repeated our analysis with three different peak thresholds for daily stomatal O₃ uptake rates above which an effect would occur and with three different delay periods over which an induced O₃ effect would last. The fact that all nine analyses produced the same outcome provides validity for our conclusions, despite the uncertainty involved in the identification of days with O₃ effects.

The lack of detected O₃ effects on GPP does not mean that O₃ did not negatively affect this Scots pine stand in Brasschaat. Stomatal O₃ uptake has been linked here to reductions in GPP only. As already stated in the Introduction, protective responses such as compensation and enhanced tolerance occur in trees (Skärby et al., 1998). It is likely that the trees at our study site were able to fully detoxify the O₃ taken up. The respiratory cost involved might have come at the expense of biomass production and growth, while gross C uptake remained unaffected. Future analyses, such as a tree ring analysis, may provide an answer to whether this is the case.

5 Summary

We parameterised a multiplicative stomatal model for a Scots pine stand in Brasschaat. This species- and site-specific parameterised model performed very well. With this model embedded in a resistance scheme, stomatal O₃ fluxes were calculated and used to test for O₃ effects on GPP. Only very small reductions in growing season GPP were calculated. Although the critical levels for AOT40 and POD₁ were exceeded in every single year, no significant correlations between total GPP residuals and stomatal O₃ flux, AOT40, and POD₁ were found. Within the limitations of the approach used in this study, we can thus conclude that O₃ did not affect the gross carbon uptake by the Scots pine stand in Brasschaat.

Data availability. Data to this paper can be found in the Supplement.

Appendix A: Gross primary productivity measurements

This study investigates O₃ effects on GPP. Below, it is briefly explained how GPP was measured.

Gross primary productivity ($\mu\text{mol C m}^{-2} \text{s}^{-1}$) was derived from net ecosystem exchange (NEE) measured with the eddy covariance technique (Baldocchi and Meyers, 1998). The eddy covariance system was set up in August 1996. It consists of a sonic anemometer (Solent 1012R2; Gill Instruments, Lymington, UK) to measure turbulence and an infrared gas analyser (IRGA) (LI-6262; LI-COR Inc., Lincoln, NE, USA) to measure the CO₂ concentration. The measurements were conducted at the top of the tower at a height of 41 m, about 19 m above the canopy. Half-hourly NEE fluxes were calculated following the guidelines of the standard EU-ROFLUX methodology (Aubinet et al., 1999) as described in detail by Carrara et al. (2003, 2004). All half-hourly fluxes originating from outside the footprint were removed according to the criteria described by Nagy et al. (2006). A detailed description of the composition of the footprint can be found in the same paper. After filtering for non-forest fluxes, the remaining data have been filtered for non-optimal turbulence conditions using the u^* approach (Aubinet et al., 1999); the method described in Reichstein et al. (2005) has been used as a basis, including bootstrapping to estimate 100 thresholds per year. After all the filtering, on average about 55 % of the half-hourly fluxes were discarded. The remaining data were used to gap-fill the missing data following the non-linear regression method (NLR; Falge et al., 2001a) and the marginal distribution sampling method (MDS; Reichstein et al., 2005). Gross primary productivity was derived from NEE by adding the modelled total ecosystem respiration (autotrophic plus heterotrophic) to NEE. The ecosystem respiration was modelled with standardised algorithms as presented in Falge et al. (2001b).

Appendix B: The multiplicative stomatal model

In this work, the multiplicative stomatal model described by Jarvis (1976) is modified specifically for the Scots pine stand in Brasschaat. The basic model is explained below.

The stomatal conductance to O₃ at needle level (g_{st}) was modelled with the multiplicative stomatal model first described by Jarvis (1976) and later reformulated by Emberson et al. (2000). In this study, we used a modified version of the model (Eq. 1):

$$g_{\text{st}} = g_{\max} \cdot f_{\text{phen}} \cdot (f_{\min} + (1 - f_{\min}) \cdot (f_{\text{PAR}} \cdot f_T \cdot f_{\text{VPD}} \cdot f_{\text{SWP}})). \quad (\text{B1})$$

Here, g_{st} is the stomatal conductance to O₃ and g_{\max} is the maximal stomatal conductance to O₃. The functions f_{PHEN} , f_{PAR} , f_T , f_{VPD} , and f_{SWP} represent the modification of g_{\max} by, respectively, phenology, PAR, T_{air} , VPD, and SWP. The function f_{\min} is the ratio of g_{\min} and g_{\max} , where g_{\min} is

the minimal stomatal conductance to O₃. Impaired stomatal aperture mechanisms (stomatal sluggishness) due to O₃ exposure (Paoletti and Grulke, 2010) were not included in this model. In this modified version, PAR, T_{air} , VPD, and SWP influence the range between g_{\max} and g_{\min} instead of g_{\max} and zero. This modification was needed to allow for a constant g_{st} during the nighttime ($= g_{\min}$) that increases as soon as $\text{PAR} > 0 \mu\text{mol m}^{-2} \text{s}^{-1}$, in accordance with our observations (Op de Beeck et al., 2010).

Phenology modifies g_{\max} because of the variation in g_{st} due to differences in needle age. The function f_{PHEN} is modelled as follows:

$$\begin{aligned} \text{if } SGS \leq \text{doy} \leq (SGS + c), \\ \text{then } f_{\text{PHEN}} = f_{\min} + (1 - f_{\min}) \\ \cdot (1 - b) \cdot \left(\frac{\text{doy} - SGS}{c} \right) + b \\ \text{if } SGS + c \leq \text{doy} \leq EGS - d, \\ \text{then } f_{\text{PHEN}} = f_{\min} + (1 - f_{\min}) \cdot 1 \\ \text{if } EGS - d \leq \text{doy} \leq EGS, \\ \text{then } f_{\text{PHEN}} = f_{\min} + (1 - f_{\min}) \\ \cdot (1 - b) \cdot \left(\frac{EGS - \text{doy}}{d} \right) + b, \end{aligned} \quad (\text{B2})$$

where SGS is the start of the growing season (doy = 115), EGS is the end of the growing season (doy = 300), and b (= 0.8), c (= 20), and d (= 20) are species-specific parameters representing the minimum of f_{PHEN} . This means the number of days for f_{PHEN} to reach its maximum and the number of days during the decline of f_{PHEN} for the minimum to be reached again, assuming a linear increase and decrease at the start and end of the growing season.

The stomatal response to PAR is described by a rectangular hyperbola, where a_{PAR} is a species-specific parameter determining the shape of the hyperbola (Emberson et al., 2000):

$$f_{\text{PAR}} = 1 - \exp(-a_{\text{PAR}} \cdot \text{PAR}). \quad (\text{B3})$$

The stomatal response to T_{air} is given by a parabolic function, where T_{\min} is the minimum temperature at which stomatal opening occurs and T_{opt} is the optimum temperature of stomatal opening (Emberson et al., 2000):

$$f_T = \max \left(0; 1 - \frac{(T - T_{\text{opt}})^2}{(T_{\text{opt}} - T_{\min})^2} \right). \quad (\text{B4})$$

The stomatal response to VPD is described by the following relationship, where VPD_{\min} is a threshold for minimal stomatal opening and VPD_{\max} is a threshold for full stomatal opening (Emberson et al., 2000):

$$f_{\text{VPD}} = \min \left(1; \max \left(0; \frac{\text{VPD}_{\min} - \text{VPD}}{\text{VPD}_{\min} - \text{VPD}_{\max}} \right) \right). \quad (\text{B5})$$

The stomatal response to SWP is described by the following relationship, where SWP_{\min} is a threshold for minimal

stomatal opening and SWP_{\max} is a threshold for full stomatal opening (Emberson et al., 2000):

$$f_{\text{SWP}} = \min \left(1; \max \left(0; \frac{\text{SWP}_{\min} - \text{SWP}}{\text{SWP}_{\min} - \text{SWP}_{\max}} \right) \right). \quad (\text{B6})$$

Appendix C: Statistics of model performance

In order to test how well the modified stomatal model performed, several model statistics were calculated. These model statistics are explained below.

The mean bias (MB) is the mean difference between the simulations (S_i) and the observations (O_i), with n being the number of data points (Stone, 1993):

$$\text{MB} = n^{-1} \sum_{i=1}^n (S_i - O_i). \quad (\text{C1})$$

The mean relative error (MRE) is the mean relative difference between the simulations and the observations (Peierls, 1935):

$$\text{MRE} = n^{-1} \sum_{i=1}^n \frac{|S_i - O_i|}{O_i}. \quad (\text{C2})$$

Willmott's index of agreement (d) is a dimensionless goodness-of-fit coefficient, with \bar{O} being the mean observation (Willmott, 1981). The index can vary between 0 and 1, with d equal to 1 for perfect agreement between the simulations and observations:

$$d = 1 - \frac{\sum_{i=1}^n (S_i - O_i)^2}{\sum_{i=1}^n (|S_i - \bar{O}| + |O_i - \bar{O}|)}. \quad (\text{C3})$$

The model efficiency (ME) gives an indication of how well the observations match the simulations (Nash and Sutcliffe, 1970). The model efficiency can range from $-\infty$ to 1 and is 1 when the simulations and observations match perfectly. An efficiency of zero indicates that the simulations are as accurate as the mean observation, and an efficiency of less than zero indicates that the mean observation is a better predictor than the model:

$$\text{ME} = 1 - \frac{\sum_{i=1}^n (S_i - O_i)^2}{\sum_{i=1}^n (O_i - \bar{O})^2}. \quad (\text{C4})$$

The root mean square error (RMSE) is a measure of the mean absolute difference between the simulations and the observations, weighting large differences heavily (Willmott et al., 1985). The systematic component (RMSE_s) estimates the model's linear or systematic error; hence, the better the regression between the simulations and observations, the smaller the systematic component (Willmott et al., 1985). The unsystematic component is a measure of how much of the discrepancy between the simulations and observations is due to random processes (Willmott et al., 1985). A good model will provide low values of RMSE, with RMSE_s close to zero and RMSE_u close to the RMSE (Willmott et al., 1985):

$$\text{RMSE} = \sqrt{n^{-1} \sum_{i=1}^n (S_i - O_i)^2} \quad (\text{C5})$$

$$\text{RMSE}_s = \sqrt{n^{-1} \sum_{i=1}^n (S'_i - O_i)^2} \quad (\text{C6})$$

$$\text{RMSE}_u = \sqrt{n^{-1} \sum_{i=1}^n (S_i - S'_i)^2}. \quad (\text{C7})$$

$S'_i = a \cdot O_i + b$, where a and b are slope and intercept, respectively, of the linear regression of the simulations versus the observations.

The Supplement related to this article is available online at doi:10.5194/bg-14-1839-2017-supplement.

Author contributions. Lore T. Verryckt, Maarten Op de Beeck, Bert Gielen, Marilyn Roland, and Ivan A. Janssens designed the study. Johan Neirynck provided the O₃ mixing ratio measurements, Bert Gielen provided the EC and LAI data, Bert Gielen, Maarten Op de Beeck, and Lore T. Verryckt measured g_{st} in situ, and Maarten Op de Beeck and Lore T. Verryckt conducted the modelling. All authors contributed to the writing.

Competing interests. The authors declare that they have no conflict of interest.

Acknowledgements. The measurements for this work were funded by the Hercules Foundation through the support of the Brasschaat ICOS ecosystem station. Ivan A. Janssens acknowledges support from the European Research Council Synergy Grant; ERC-2013-SyG-610028 IMBALANCE-P.

Edited by: I. Trebs

Reviewed by: five anonymous referees

References

- Ainsworth, E. A., Yendrek, C. R., Sitch, S., Collins, W. J., and Emberson, L. D.: The Effects of Tropospheric Ozone on Net Primary Productivity and Implications for Climate Change, *Annu. Rev. Plant Biol.*, 63, 637–661, doi:10.1146/annurev-applant-042110-103829, 2012.
- Akhand, K., Nizamuddin, M., Roystman, L., and Kogan, F.: Using remote sensing satellite data and artificial neural network for prediction of potato yield in Bangladesh, *Proc. SPIE*, 9975, 997508, doi:10.1117/12.2237214, 2016.
- Altimir, N., Tuovinen, J.-P., Vesala, T., Kulmala, M., and Hari, P.: Measurements of ozone removal by Scots pine shoots: calibration of a stomatal uptake model including the non-stomatal component, *Atmos. Environ.*, 38, 2387–2398, doi:10.1016/j.atmosenv.2003.09.077, 2004.
- Ashmore, M. R.: Assessing the future global impacts of ozone on vegetation, *Plant Cell Environ.*, 28, 949–964, doi:10.1111/j.1365-3040.2005.01341.x, 2005.
- Aubinet, M., Grelle, A., Ibrom, A., Rannik, Ü., Moncrieff, J., Foken, T., Kowalski, A. S., Martin, P. H., Berbigier, P., Bernhofer, C., Clement, R., Elbers, J., Granier, A., Grünwald, T., Morgenstern, K., Pilegaard, K., Rebmann, C., Snijders, W., Valentini, R., and Vesala, T.: Estimates of the Annual Net Carbon and Water Exchange of Forests: The EUROFLUX Methodology, in: *Adv. Ecol. Res.*, edited by: Fitter, A. H. and Raffaelli, D. G., Academic Press, 113–175, 1999.
- Baldocchi, D. and Meyers, T.: On using eco-physiological, micrometeorological and biogeochemical theory to evaluate carbon dioxide, water vapor and trace gas fluxes over vegetation: a perspective, *Agr. Forest Meteorol.*, 90, 1–25, doi:10.1016/S0168-1923(97)00072-5, 1998.
- Baldocchi, D. D., Hicks, B. B., and Camara, P.: A canopy stomatal resistance model for gaseous deposition to vegetated surfaces, *Atmos. Environ.*, 21, 91–101, doi:10.1016/0004-6981(87)90274-5, 1987.
- Beedlow, P. A., Tingey, D. T., Phillips, D. L., Hogsett, W. E., and Olszyk, D. M.: Rising atmospheric CO₂ and carbon sequestration in forests, *Front. Ecol. Environ.*, 2, 315–322, 2004.
- Büker, P., Feng, Z., Uddling, J., Briolat, A., Alonso, R., Braun, S., Elvira, S., Gerosa, G., Karlsson, P. E., Le Thiec, D., Marzuoli, R., Mills, G., Oksanen, E., Wieser, G., Wilkinson, M., and Emberson, L. D.: New flux based dose-response relationships for ozone for European forest tree species, *Environ. Pollut.*, 206, 163–174, doi:10.1016/j.envpol.2015.06.033, 2015.
- Carrara, A., Kowalski, A. S., Neirynck, J., Janssens, I. A., Yuste, J. C., and Ceulemans, R.: Net ecosystem CO₂ exchange of mixed forest in Belgium over 5 years, *Agr. Forest Meteorol.*, 119, 209–227, doi:10.1016/s0168-1923(03)00120-5, 2003.
- Carrara, A., Janssens, I. A., Curiel Yuste, J., and Ceulemans, R.: Seasonal changes in photosynthesis, respiration and NEE of a mixed temperate forest, *Agr. Forest Meteorol.*, 126, 15–31, doi:10.1016/j.agrformet.2004.05.002, 2004.
- Cieslik, S. A.: Ozone uptake by various surface types: a comparison between dose and exposure, *Atmos. Environ.*, 38, 2409–2420, doi:10.1016/j.atmosenv.2003.10.063, 2004.
- CLRTAP: Mapping Critical Levels for Vegetation, Chapter III of Manual on methodologies and criteria for modelling and mapping critical loads and levels and air pollution effects, risks and trends, UNECE Convention on Long-range Transboundary Air Pollution, available at: www.icpmapping.org (last access: 28 March 2017), 2015.
- Dizengremel, P.: Effects of ozone on the carbon metabolism of forest trees, *Plant Physiol. Biochem.*, 39, 729–742, doi:10.1016/S0981-9428(01)01291-8, 2001.F
- Dyer, A. J.: A review of flux-profile relationships, *Bound.-Lay. Meteorol.*, 7, 363–372, doi:10.1007/bf00240838, 1974.
- EEA (European Environment Agency): available at: <http://www.eea.europa.eu/>, last access: 1 May 2014.
- Emberson, L. D., Ashmore, M. R., Cambridge, H. M., Simpson, D., and Tuovinen, J. P.: Modelling stomatal ozone flux across Europe, *Environ. Pollut.*, 109, 403–413, 2000.
- Emberson, L. D., Büker, P., and Ashmore, M. R.: Assessing the risk caused by ground level ozone to European forest trees: a case study in pine, beech and oak across different climate regions, *Environ. Pollut.*, 147, 454–466, doi:10.1016/j.envpol.2006.10.026, 2007.
- Falge, E., Baldocchi, D., Olson, R., Anthoni, P., Aubinet, M., Bernhofer, C., Burba, G., Ceulemans, R., Clement, R., Dolman, H., Granier, A., Gross, P., Grünwald, T., Hollinger, D., Jensen, N.-O., Katul, G., Keronen, P., Kowalski, A., Lai, C. T., Law, B. E., Meyers, T., Moncrieff, J., Moors, E., Munger, J. W., Pilegaard, K., Rannik, Ü., Rebmann, C., Suyker, A., Tenhunen, J., Tu, K., Verma, S., Vesala, T., Wilson, K., and Wofsy, S.: Gap filling strategies for defensible annual sums of net ecosystem exchange, *Agr. Forest Meteorol.*, 107, 43–69, doi:10.1016/S0168-1923(00)00225-2, 2001a.
- Falge, E., Baldocchi, D., Olson, R., Anthoni, P., Aubinet, M., Bernhofer, C., Burba, G., Ceulemans, R., Clement, R., Dolman, H., Granier, A., Gross, P., Grünwald, T., Hollinger, D., Jensen, N.-O., Katul, G., Keronen, P., Kowalski, A., Ta Lai, C., Law, B.

- E., Meyers, T., Moncrieff, J., Moors, E., Munger, J. W., Pilegaard, K., Rannick, Ü., Rebmann, C., Suyker, A., Tenhunen, J., Tu, K., Verma, S., Vesala, T., Wilson, K., and Wofsy, S.: Gap filling strategies for long term energy flux data sets, *Agr. Forest Meteorol.*, 107, 71–77, 2001b.
- Fares, S., McKay, M., Holzinger, R., and Goldstein, A. H.: Ozone fluxes in a *Pinus ponderosa* ecosystem are dominated by non-stomatal processes: Evidence from long-term continuous measurements, *Agr. Forest Meteorol.*, 150, 420–431, doi:10.1016/j.agrformet.2010.01.007, 2010.
- Fares, S., Vargas, R., Dett, M., Goldstein, A. H., Karlik, J., Paoletti, E., and Vitale, M.: Tropospheric ozone reduces carbon assimilation in trees: estimates from analysis of continuous flux measurements, *Glob. Change Biol.*, 19, 2427–2443, doi:10.1111/gcb.12222, 2013.
- Gerola, G., Vitale, M., Finco, A., Manes, F., Denti, A., and Cieslik, S.: Ozone uptake by an evergreen Mediterranean Forest (*Quercus ilex*) in Italy. Part I: Micrometeorological flux measurements and flux partitioning, *Atmos. Environ.*, 39, 3255–3266, doi:10.1016/j.atmosenv.2005.01.056, 2005.
- Gielen, B., Verbeeck, H., Neirynck, J., Sampson, D. A., Vermeiren, F., and Janssens, I. A.: Decadal water balance of a temperate Scots pine forest (*Pinus sylvestris* L.) based on measurements and modelling, *Biogeosciences*, 7, 1247–1261, doi:10.5194/bg-7-1247-2010, 2010.
- Gielen, B., Neirynck, J., Luyssaert, S., and Janssens, I. A.: The importance of dissolved organic carbon fluxes for the carbon balance of a temperate Scots pine forest, *Agr. Forest Meteorol.*, 151, 270–278, doi:10.1016/j.agrformet.2010.10.012, 2011.
- Gielen, B., De Vos, B., Campioli, M., Neirynck, J., Papale, D., Verstraeten, A., Ceulemans, R., and Janssens, I. A.: Biometric and eddy covariance-based assessment of decadal carbon sequestration of a temperate Scots pine forest, *Agr. Forest Meteorol.*, 174–175, 135–143, doi:10.1016/j.agrformet.2013.02.008, 2013.
- Gond, V., De Pury, D. G. G., Veroustraete, F., and Ceulemans, R.: Seasonal variations in leaf area index, leaf chlorophyll, and water content; scaling-up to estimate fAPAR and carbon balance in a multilayer, multispecies temperate forest, *Tree Physiol.*, 19, 673–679, 1999.
- Grinhage, L.: An O₃ flux-based risk assessment for spring wheat, Background Document, Joint ICP Vegetation/EMEP, Ad-hoc Expert Panel Meeting on Modelling and Mapping of Ozone Flux and Deposition to Vegetation, UNECE Convention on Long-range Transboundary Air Pollution, 16–19 June 2002, Harrogate, UK, 2002.
- Grüters, U., Fangmeier, A., and Jäger, H.-J.: Modelling stomatal responses of spring wheat (*Triticum aestivum* L. cv. Turbo) to ozone and different levels of water supply, *Environ. Pollut.*, 87, 141–149, 1995.
- Huttunen, S. and Manninen, S.: A review of ozone responses in Scots pine (*Pinus sylvestris*), *Environ. Exp. Bot.*, 90, 17–31, doi:10.1016/j.envexpbot.2012.07.001, 2013.
- ICP Vegetation: Yield response and ozone injury on *Phaseolus vulgaris*: Experimental Protocol, ICP Vegetation Programme Coordination Centre, CEH Bangor, UK, 2011.
- IPCC: Climate Change 2007: Synthesis Report. Contribution to Working Group I, II and III to the Fourth Assessment Report of the Intergovernmental Panel on Climate Change, Geneva, Switzerland, 104 pp., 2007.
- Janssens, I. A., Sampson, D. A., Cermak, J., Meiresonne, L., Riguzzi, F., Overloop, S., and Ceulemans, R.: Above- and belowground pythomass and carbon storage in a Belgian Scots pine stand, *Ann. For. Sci.*, 56, 81–90, 1999.
- Jarvis, P. G.: The interpretation of the variations in leaf water potential and stomatal conductance found in canopies in the field, *Philos. T. R. Soc. B*, 273, 593–610, 1976.
- Jonckheere, I., Muys, B., and Coppin, P.: Allometry and evaluation of in situ optical LAI determination in Scots pine: a case study in Belgium, *Tree Physiol.*, 25, 723–732, 2005.
- Karlsson, P. E., Uddling, J., Braun, S., Broadmeadow, M., Elvira, S., Gimeno, B. S., Le Thiec, D., Oksanen, E., Vandermeiren, K., Wilkinson, M., and Emberson, L.: New critical levels for ozone effects on young trees based on AOT40 and simulated cumulative leaf uptake of ozone, *Atmos. Environ.*, 38, 2283–2294, doi:10.1016/j.atmosenv.2004.01.027, 2004.
- Karlsson, P. E., Braun, S., Broadmeadow, M., Elvira, S., Emberson, L., Gimeno, B. S., Le Thiec, D., Novak, K., Oksanen, E., Schaub, M., Uddling, J., and Wilkinson, M.: Risk assessments for forest trees: the performance of the ozone flux versus the AOT concepts, *Environ. Pollut.*, 146, 608–616, doi:10.1016/j.envpol.2006.06.012, 2007.
- Konôpka, B., Yuste, J. C., Janssens, I. A., and Ceulemans, R.: Comparison of Fine Root Dynamics in Scots Pine and Pedunculate Oak in Sandy Soil, *Plant Soil*, 276, 33–45, doi:10.1007/s11104-004-2976-3, 2005.
- Lek, S. and Guegan, J. F.: Artificial neural networks as a tool in ecological modelling, an introduction, *Ecol. Model.*, 120, 65–73, doi:10.1016/S0304-3800(99)00092-7, 1999.
- Li, P., Calatayud, V., Gao, F., Uddling, J., and Feng, Z.: Differences in ozone sensitivity among woody species are related to leaf morphology and antioxidant levels, *Tree Physiol.*, 36, 1105–1116, doi:10.1093/treephys/tpw042, 2016.
- Liu, S., Zhuang, Q., He, Y., Noormets, A., Chen, J., and Gu, L.: Evaluating atmospheric CO₂ effects on gross primary productivity and net ecosystem exchanges of terrestrial ecosystems in the conterminous United States using the AmeriFlux data and an artificial neural network approach, *Agr. Forest Meteorol.*, 220, 38–49, doi:10.1016/j.agrformet.2016.01.007, 2016.
- Marquardt, D.: An Algorithm for Least-Squares Estimation of Nonlinear Parameters, *J. Soc. Ind. Appl. Math.*, 11, 431–441, doi:10.1137/0111030, 1963.
- Matyssek, R. and Sandermann, H.: Impact of Ozone on Trees: an Ecophysiological Perspective, in: *Progress in Botany: Genetics Physiology Systematics Ecology*, edited by: Esser, K., Lüttge, U., Beyschlag, W., and Hellwig, F., Springer, Berlin Heidelberg, 349–404, 2003.
- Mauzerall, D. L. and Wang, X.: Protecting agricultural crops from the effects of tropospheric ozone exposure: Reconciling Science and Standard Setting in the United States, Europe, and Asia, *Annu. Rev. Energ. Env.*, 26, 237–268, doi:10.1146/annurev.energy.26.1.237, 2001.
- McLaughlin, S. B., Nosal, M., Wullschleger, S. D., and Sun, G.: Interactive effects of ozone and climate on tree growth and water use in a southern Appalachian forest in the USA, *New Phytol.*, 174, 109–124, doi:10.1111/j.1469-8137.2007.02018.x, 2007.
- Mikkelsen, T. N., Ro-Poulsen, H., Hovmand, M. F., Jensen, N. O., Pilegaard, K., and Egeløv, A. H.: Five-year measurements of

- ozone fluxes to a Danish Norway spruce canopy, *Atmos. Environ.*, 38, 2361–2371, doi:10.1016/j.atmosenv.2003.12.036, 2004.
- Musselman, R. C. and Massman, W. J.: Ozone flux to vegetation and its relationship to plant response and ambient air quality standards, *Atmos. Environ.*, 33, 65–73, 1999.
- Nagy, M. T., Janssens, I. A., Curiel Yuste, J., Carrara, A., and Ceulemans, R.: Footprint-adjusted net ecosystem CO₂ exchange and carbon balance components of a temperate forest, *Agr. Forest Meteorol.*, 139, 344–360, doi:10.1016/j.agrformet.2006.08.012, 2006.
- Nash, J. E. and Sutcliffe, J. V.: River flow forecasting through conceptual models, *J. Hydrol.*, 10, 282–290, 1970.
- Neirynck, J., Janssens, I. A., Roskams, P., Quataert, P., Verschelde, P., and Ceulemans, R.: Nitrogen biogeochemistry of a mature Scots pine forest subjected to high nitrogen loads, *Biogeochemistry*, 91, 201–222, doi:10.1007/s10533-008-9280-x, 2008.
- Neirynck, J., Gielen, B., Janssens, I. A., and Ceulemans, R.: Insights into ozone deposition patterns from decade-long ozone flux measurements over a mixed temperate forest, *J. Environ. Monitor*, 14, 1684–1695, doi:10.1039/c2em10937a, 2012.
- Op de Beeck, M., Gielen, B., Jonckheere, I., Samson, R., Janssens, I. A., and Ceulemans, R.: Needle age-related and seasonal photosynthetic capacity variation is negligible for modelling yearly gas exchange of a sparse temperate Scots pine forest, *Biogeosciences*, 7, 199–215, doi:10.5194/bg-7-199-2010, 2010.
- Paoletti, E. and Grulke, N. E.: Ozone exposure and stomatal sluggishness in different plant physiognomic classes, *Environ. Pollut.*, 158, 2664–2671, doi:10.1016/j.envpol.2010.04.024, 2010.
- Peierls, R.: Statistical Error in Counting Experiments, *P. Roy. Soc. A-Math. Phys.*, 149, 467–486, doi:10.1098/rspa.1935.0076, 1935.
- Reichstein, M., Falge, E., Baldocchi, D., Papale, D., Aubinet, M., Berbigier, P., Bernhofer, C., Buchmann, N., Gilmanov, T., Granier, A., Grünwald, T., Havránková, K., Ilvesniemi, H., Janous, D., Knöhl, A., Laurila, T., Lohila, A., Loustau, D., Matteucci, G., Meyers, T., Miglietta, F., Ourcival, J.-M., Pumpanen, J., Rambal, S., Rotenberg, E., Sanz, M., Tenhunen, J., Seufert, G., Vaccari, F., Vesala, T., Yakir, D., and Valentini, R.: On the separation of net ecosystem exchange into assimilation and ecosystem respiration: review and improved algorithm, *Glob. Change Biol.*, 11, 1424–1439, doi:10.1111/j.1365-2486.2005.001002.x, 2005.
- Rochelle-Newall, E. J., Winter, C., Barrón, C., Borges, A. V., Duarte, C. M., Elliott, M., Frankignoulle, M., Gazeau, F., Middelburg, J. J., Pizay, M.-D., and Gattuso, J.-P.: Artificial neural network analysis of factors controlling ecosystem metabolism in coastal systems, *Ecol. Appl.*, 17, S185–S196, 2007.
- Samuelson, L. J.: Ozone-exposure responses of Black-Cherry and Red Maple seedlings, *Environ. Exp. Bot.*, 34, 355–362, doi:10.1016/0098-8472(94)90017-5, 1994.
- Simpson, D., Ashmore, M. R., Emberson, L., and Tuovinen, J. P.: A comparison of two different approaches for mapping potential ozone damage to vegetation. A model study, *Environ. Pollut.*, 146, 715–725, doi:10.1016/j.envpol.2006.04.013, 2007.
- Skärby, L., Troeng, E., and Boström, C. A.: Ozone uptake and effects on transpiration, net photosynthesis and dark respiration in Scots pine, *Forest Sci.*, 33, 801–808, 1987.
- Skärby, L., Ro-Poulsen, H., Wellburn, F. A. M., and Sheppard, L. J.: Impacts of ozone on forests: a European perspective, *New Phytol.*, 139, 109–122, 1998.
- Stone, R. J.: Improved statistical procedure for the evaluation of solar radiation estimation models, *Sol. Energy*, 51, 289–291, 1993.
- Subramanian, N., Karlsson, P. E., Bergh, J., and Nilsson, U.: Impact of Ozone on Sequestration of Carbon by Swedish Forests under a Changing Climate: A Modeling Study, *Forest Sci.*, 61, 445–457, doi:10.5849/forsci.14-026, 2015.
- van Genuchten, M. T.: A Closed-form Equation for Predicting the Hydraulic Conductivity of Unsaturated Soils, *Soil Sci. Soc. Am. J.*, 44, 892–898, doi:10.2136/sssaj1980.03615995004400050002x, 1980.
- Vitale, M., Gerosa, G., Ballarindenti, A., and Manes, F.: Ozone uptake by an evergreen mediterranean forest (*Quercus ilex* L.) in Italy – Part II: flux modelling. Upscaling leaf to canopy ozone uptake by a process-based model, *Atmos. Environ.*, 39, 3267–3278, doi:10.1016/j.atmosenv.2005.01.057, 2005.
- Willmott, C. J.: On the validation of models, *Phys. Geogr.*, 2, 184–194, 1981.
- Willmott, C. J., Ackleson, S. G., Davis, R. E., Feddema, J. J., Klink, K. M., Legates, D. R., O'Donnell, J., and Rowe, C. M.: Statistics for the evaluation and comparison of models, *J. Geophys. Res.*, 90, 8995–9005, 1985.
- Wittig, V. E., Ainsworth, E. A., Naidu, S. L., Karnosky, D. F., and Long, S. P.: Quantifying the impact of current and future tropospheric ozone on tree biomass, growth, physiology and biochemistry: a quantitative meta-analysis, *Glob. Change Biol.*, 15, 396–424, doi:10.1111/j.1365-2486.2008.01774.x, 2009.
- Young, P. J., Archibald, A. T., Bowman, K. W., Lamarque, J.-F., Naik, V., Stevenson, D. S., Tilmes, S., Voulgarakis, A., Wild, O., Bergmann, D., Cameron-Smith, P., Cionni, I., Collins, W. J., Dalgaard, S. B., Doherty, R. M., Eyring, V., Faluvegi, G., Horowitz, L. W., Josse, B., Lee, Y. H., MacKenzie, I. A., Nagashima, T., Plummer, D. A., Righi, M., Rumbold, S. T., Skeie, R. B., Shindell, D. T., Strode, S. A., Sudo, K., Szopa, S., and Zeng, G.: Pre-industrial to end 21st century projections of tropospheric ozone from the Atmospheric Chemistry and Climate Model Intercomparison Project (ACCMIP), *Atmos. Chem. Phys.*, 13, 2063–2090, doi:10.5194/acp-13-2063-2013, 2013.
- Yue, X. and Unger, N.: Ozone vegetation damage effects on gross primary productivity in the United States, *Atmos. Chem. Phys.*, 14, 9137–9153, doi:10.5194/acp-14-9137-2014, 2014.
- Yuste, J. C., Konôpka, B., Janssens, I. A., Coenen, K., Xiao, C. W., and Ceulemans, R.: Contrasting net primary productivity and carbon distribution between neighboring stands of *Quercus robur* and *Pinus sylvestris*, *Tree Physiol.*, 25, 701–712, 2005.
- Zapletal, M., Cudlin, P., Chroust, P., Urban, O., Pokorný, R., Edwards-Jonasova, M., Czerny, R., Janous, D., Tufarova, K., Vecera, Z., Mikuska, P., and Paoletti, E.: Ozone flux over a Norway spruce forest and correlation with net ecosystem production, *Environ. Pollut.*, 159, 1024–1034, doi:10.1016/j.envpol.2010.11.037, 2011.
- Zona, D., Gioli, B., Fares, S., De Groote, T., Pilegaard, K., Ibrom, A., and Ceulemans, R.: Environmental controls on ozone fluxes in a poplar plantation in Western Europe, *Environ. Pollut.*, 184, 201–210, doi:10.1016/j.envpol.2013.08.032, 2014.